Waste Management 212 (2026) 115349

Contents lists available at ScienceDirect

Waste Management

journal homepage: www.elsevier.com/locate/wasman

Research Paper

Waste–to–waste valorization: Sustainable palladium recovery from real spent catalytic converter leachates using chicken feathers

Amir Nobahar [a], Flavia N. Braga [a,b], Filipe H.B. Sosa [a], Nicolas Schaeffer [a], João A.P. Coutinho [a], Helena Passos [b,*]

[a] CICECO – Aveiro Institute of Materials, Department of Chemistry, University of Aveiro, Aveiro 3810–193, Portugal
[b] LSRE-LCM, ALiCE, Faculty of Engineering, University of Porto, Rua Dr. Roberto Frias, Porto 4200-465, Portugal

ARTICLE INFO

Keywords:
Precious metal recovery
Waste valorization
Spent catalytic converter
Platinum group metals (PGM)
Selective adsorption
Keratin biosorbent

ABSTRACT

The increasing demand for platinum group metals (PGM), mainly driven by their extensive use in automotive catalytic converters, has heightened the need for efficient and green recovery methods. Simultaneously, the poultry industry generates significant amounts of keratin–rich chicken feathers (CF), which are commonly disposed of by incineration or landfilling, raising environmental concerns. This study explores the use of CF as a sustainable and cost–effective biosorbent for the selective recovery of Pd from synthetic multimetallic solutions and HCl–based spent autocatalytic converters leachates. Adsorption experiments revealed that the optimal Pd uptake (14.10 ± 0.31) mg.g^{-1} was achieved at 0.2 M HCl (pH ~ 0.79), while 2 M HCl provided the highest selectivity towards Pd over other metals. Adsorption kinetics followed a pseudo–second–order model, indicating chemisorption as the dominant mechanism, and Langmuir isotherm analysis yielded a Pd adsorption capacity of (19.61 ± 1.31) mg.g^{-1}. Desorption tests demonstrated ~100% Pd recovery using 0.2 M thiourea + 0.5 M HCl solution. Characterization of the CF by Raman and solid–state UV–Vis spectroscopy, FTIR, SEM−EDX, and XPS confirmed the interaction of Pd with disulfide bonds and protonated amino groups as Pd–chloride complexes. Bench–scale trials on HCl–based leachates with an optimized CF to leachate ratio achieved near–complete Pd separation in a single adsorption step with high purity, highlighting the robustness and selectivity of this method under realistic conditions. Pd was successfully desorbed from CF by acidified thiourea solution, offering added value for catalytic applications.

1. Introduction

Platinum group metals (PGMs) such as Pt, Pd, and Rh are indispensable in catalysis, chemical processing, electronics, and emerging hydrogen technologies, yet their natural availability is extremely limited (Chaudhuri et al., 2023b). The automotive industry, as the largest consumer of PGM, uses PGM in catalytic converters to reduce harmful emissions (Shukla et al., 2023). According to a report by The Business Research Company (2025), the global automotive catalytic converter market was valued at about US$176 billion in 2024 and is projected to reach roughly US$279 billion by 2029, with an annual growth rate of 9.9%. Consequently, effective waste management strategies are critical to ensure the sustainable recovery and recycling of these valuable metals. End–of–life catalytic converters, commonly known as spent autocatalytic converters (SACC), are valuable secondary sources of PGM, with concentrations ranging from 140 to 12,000 ppm, significantly higher than the 1–10 ppm typically found in natural ores (Saguru et al., 2018). Yet, by 2020, recycling of SACC accounted for only about 25% of the total supply worldwide, hindered by challenges such as the absence of standardized processes, environmental concerns, and reliance on energy–intensive methods (Trinh et al., 2020).

Recovery of PGM from SACC typically involves pyro– or hydrometallurgical processes, with hydrometallurgical methods preferred due to their lower costs and improved environmental sustainability (Grilli et al., 2023). In hydrometallurgical processes, SACC are first leached with an acid such as HCl, followed by the separation of PGM through different methods. Emerging green methods, such as PGM adsorption to biobased advanced structures (Kim and Hong, 2024; Mincke et al., 2019; Wang et al., 2021), bacterial–mediated reduction (Murray et al., 2017), secondary plant metabolites (Nobahar et al., 2021), algal–mediated recovery (Saitoh et al., 2017), and protein–assisted recovery (Bongers et al., 1988) offer promising and eco–friendly alternatives to

* Corresponding author.
E-mail address: hpassos@fe.up.pt (H. Passos).

https://doi.org/10.1016/j.wasman.2026.115349
Received 6 October 2025; Received in revised form 6 January 2026; Accepted 9 January 2026
Available online 15 January 2026

conventional separation techniques. However, industrial implementation remains limited for several reasons. These include low metal recovery rates compared to conventional methods, limited selectivity in complex multimetallic solutions, scalability challenges, instability of biobased materials under harsh acidic conditions, prolonged processing times, and the high cost of bioprocess optimization (Grilli et al., 2023). Therefore, the recovery of PGM from SACC leachates still relies on traditional methods like adsorption, solvent extraction, chemical precipitation, and ion exchange, involving hazardous reagents that entail significant environmental, safety, and cost–related drawbacks (Xia and Ghahreman, 2023). Among the available separation routes, adsorption has gained increasing attention for metal recovery due to its simplicity, low reagent and energy demand, and high efficiency at low metal concentrations (Chaudhuri et al., 2016; Il Yoon et al., 2023).

An innovative and sustainable alternative to conventional adsorbents is the use of chicken feathers (CF), a major waste stream from the poultry industry. Annually, large quantities of CF, an estimated 7 to 14 million tons, are generated as waste from the poultry industry (FAO, 2023; Grazziotin et al., 2006) and are generally disposed of through landfilling and incineration, practices that contribute to environmental pollution (Tesfaye et al., 2017). CF are rich in keratin, a robust biopolymer endowed with amino, amide, disulfide, carboxyl, hydroxyl, and thiol functional groups (Sadeghi et al., 2019; Škerget et al., 2023). These functional groups exhibit the potential to interact with positively or negatively charged metal ions and complexes via electrostatic interactions, van der Waals forces, reduction processes, and physical entrapment, as proposed in existing research (Akioka et al., 2021; Chen et al., 2025; Dhaouadi et al., 2020; Shan et al., 2024; Solís-Moreno et al., 2021). With an isoelectric point of 4.4 (Škerget et al., 2023), keratin's functional groups are neutral or negatively charged in alkaline conditions, while at low pH, amino groups accept protons and become positively charged. These pH–sensitive sites allow CF to capture various metals, including positively charged metal ions of Pb, Cd, Ni, Cu, and U under slightly acidic to alkaline conditions (Chakraborty et al., 2020; Chen et al., 2021; Dhaouadi et al., 2020; Shan et al., 2024; Solís-Moreno et al., 2021).

However, research on keratin–based adsorption of negatively charged metal complexes, such as those of precious metals, remains limited (Akioka et al., 2021; Chen et al., 2025; Enkhzaya et al., 2020; Ishikawa and Suyama, 1998; Maruyama et al., 2014; Suyama et al., 1996). These materials show promising capacities ranging from 85 to 322 $mg.g^{-1}$ for Au and 30 to 87 $mg.g^{-1}$ for Pt and Pd in single–metal systems (Chen et al., 2025; Ishikawa and Suyama, 1998; Suyama et al., 1996). However, most of these studies explore PGM adsorption under idealized conditions, and they rarely evaluate the selective recovery of PGM from complex multimetallic solutions or real leachates, such as those from spent catalytic converters. Therefore, the applicability of these otherwise potent adsorbents has so far remained confined to laboratory studies rather than real hydrometallurgical operations.

To overcome these limitations, this study investigates keratin–based sorption under realistic process conditions, focusing specifically on selective Pd recovery in chloride-rich media. A waste–to–waste valorization route is implemented using unmodified CF, and their performance is assessed in multimetallic systems and real SACC leachates. Adsorption behavior is systematically analyzed across operational variables relevant to hydrometallurgical practice, and desorption is evaluated for complete and near–pure Pd recovery from the loaded CF. Mechanistic insights are obtained from a combined spectroscopic and microscopic dataset to identify the dominant Pd–keratin interaction pathways. Finally, these findings are integrated into a process–oriented workflow for Pd isolation from real HCl–based catalytic-converter leachates.

2. Experimental

A detailed description of the reagents and experimental techniques to characterize the adsorbent used in this work is provided in the "Methodology" section of SI.

2.1. Preparation of adsorbent

CF were washed three times with soapy water and dried at 50 °C in an air oven (Carbolite Gero) for 72 h. After drying, they were immersed in 99 wt% ethanol for 24 h. The cleaned CF were dried at 50 °C for 24 h. This pretreatment protocol, reported in the literature as highly effective for lipid removal from feathers, ensured efficient defatting (Mattiello et al., 2022; Polesca et al., 2023). Finally, CF were milled with a coffee grinder and stored in the refrigerator at 5 °C to prevent microbial growth, oxidation, and structural degradation of the keratin matrix (Li, 2019). Particle size distribution of CF is presented in SI Section 1.2.

2.2. Batch adsorption studies with synthetic solutions

Batch adsorption tests were conducted in 60 mL plastic jars containing 10 mL of a synthetic multi–metal solution (Fe, Zn, Ce, Pt, Pd, Rh, each 15 ± 1 $mg.L^{-1}$) with 0.2 M HCl, and 1 $g.L^{-1}$ of CF, stirred at 150 rpm and maintained at 303 K, for 6 h, unless specified otherwise. All experiments were performed in triplicate, except kinetic studies, which were conducted in duplicate. A control sample without CF, with the same number of replicates, was included in all tests to account for non–adsorptive losses. The influence of HCl molarity on PGM adsorption was examined by varying HCl concentration from 0.04 to 2.0 M. Counter anion effects were tested by adding HNO_3 or H_2SO_4 (0.2, 0.5 and 1.0 M) to solutions containing metals and 0.2 M HCl. Contact time experiments were conducted for 48 h, in 500 mL Erlenmeyer flasks with an initial solution volume of 250 mL; at predetermined time intervals, 2 mL of the solution was sampled, filtered, and analyzed. Temperature effects were studied at 303, 313, and 323 K with an accuracy of ±1 K throughout the tests, under otherwise identical conditions. Effect of initial metal concentration was studied by performing adsorption studies in metal mixture solutions containing 5, 10, 15, 25 and 35 $mg.L^{-1}$ of each metal. Effect of competitive metal ions was assessed by increasing one metal's concentration to 150 $mg.L^{-1}$ while maintaining others at 15 $mg.L^{-1}$, to observe their impact on Pd uptake.

2.3. Preparation and leaching of SACC

All the catalysts were primarily dismantled by cutting through the metallic shell and tubes with a metal saw, allowing access to the ceramic honeycombs. These honeycombs were manually broken into smaller fragments, which were then ground using a mortar and pestle to reduce their size. To achieve finer particles, materials were further milled using a Mini Mill Pulverisette 23. The prepared catalyst powders, including catalysts 1, 2, 3, and 4, were mixed in equal weight ratios to produce a homogeneous powder, referred to as MixC. Additionally, catalyst 1 alone (Volkswagen Golf III (1991–1999 production model)), hereafter as VW90, was used along with MixC for subsequent leaching experiments. The leaching procedure followed the method described by Paiva et al. (2022). Briefly, the process was performed using 11.6 M HCl with 1% H_2O_2 at 60 °C, maintaining a liquid–to–solid ratio of 2 $L.kg^{-1}$ under continuous stirring for 3 h. After leaching, the resulting solutions were separated from the solid residues and filtered. The obtained leachates were then diluted 1/6 and 1/60 (v/v) to obtain solutions with 2 M and 0.2 M HCl. Finally, the metal concentrations in both the original and diluted leachates were analyzed.

2.4. Adsorption/desorption from leachates

The diluted leachates were utilized for these tests, applying all optimized conditions derived from studies with synthetic solutions. The parameters included a contact time of 6 h, a temperature of 303 K, and HCl concentrations of 0.2 M (for highest Pd adsorption capacity) and 2.0 M (for highest selectivity). In tests with 1/60 (v/v) diluted leachates,

1 g.L^{-1} of CF was used as the adsorbent. In the tests with 1/6 (v/v) diluted leachates, adsorption was carried out through three to five consecutive adsorption cycles, using 5 g.L^{-1} of fresh CF in each cycle for MixC and VW90 leachates, respectively. Following adsorption, CF were subjected to desorption using a 0.2 M thiourea solution containing 0.5 M HCl at a CF loading of 5 g.L^{-1}.

2.5. Metal quantification

After each test, samples were filtered using PTFE syringe filters with a pore size of 0.22 µm and a diameter of 13 mm (Branchia, product code SFPT–122–100) prior to analysis. Concentration of Fe, Zn and Ce were quantified by TXRF using a Picofox S2 (Bruker Nano (Billerica, MA, USA)) with a molybdenum X–ray source. Quartz sample carriers were pretreated with 10 µL of silicon in an isopropanol solution and dried at (353 ± 1) K for at least 15 min. Samples were diluted in 1 g of a poly (vinyl alcohol) solution (0.5 wt%) and spiked with 10 µL of yttrium standard. Ten microliters of each sample were added to the pretreated quartz carrier and dried on a hot plate at (353 ± 1) K for at least 10 min. Spectra acquisition time was set to 300 s.

For Pd and Rh, TXRF is not suitable because their peaks appear in the same spectral region as Cl, whose intense signal overlaps and masks them, preventing reliable quantification. Therefore, concentrations of Pd, Pt, and Rh were determined using inductively coupled plasma–optical emission spectrometry (ICP–OES) on an iCAP 7400 system (Thermo Scientific), equipped with a nebulizing system and optical emission detection. Samples were diluted appropriately to ensure measurements fell within the calibration range (0.005–10 mg.L^{-1}) and were analyzed in triplicate for accuracy.

The adsorption capacity, q_e (mg.g^{-1}), was calculated by Equation (1):

$$q_e = \frac{(C_0 - C_e).V}{w} \quad (1)$$

The adsorption percentage, R (%), was determined using the following equation (2):

$$\%R = \frac{(C_0 - C_e)}{C_0} \times 100 \quad (2)$$

where C_0 (mg.L^{-1}) is the initial adsorbate concentration, C_e (mg.L^{-1}) is the adsorbate concentration at equilibrium, V (L) is the volume of solution, and w (g) is the mass of adsorbent.

3. Results and discussion

Preliminary experiments revealed that CFs exhibit a pronounced preference for Pd, with uptake markedly higher than for Pt, while Rh and the non−PGMs showed only minor adsorption. This indicates that CF binding sites display a strong and selective affinity toward Pd. To further investigate the potential of CF for selective PGM separation and recovery from HCl–based matrices, particularly focusing on adsorption and desorption optimization, comprehensive studies were conducted as outlined below. Unless otherwise specified, all optimization tests in Sections 3.1–3.2 and SI Sections 2.1–2.4 were conducted using a synthetic multimetallic solution containing Pd, Pt, Rh, Fe, Zn, and Ce (each at 15 ± 1 mg.L^{-1}). These metals were identified due to their prevalence in real SACC leachates.

3.1. Adsorption kinetics and effect of initial metal concentration on adsorption capacities

The adsorption behavior of metals onto CF (1 g.L^{-1}) was evaluated over a 48–h period. Results indicated that maximum uptake capacity was reached within 360 min for Pd, Pt, and Rh, after which adsorption leveled off into a plateau (Fig. 1–A). Kinetic data were analyzed using nonlinear pseudo–first–order (Lagergren, 1898) and pseudo–second–order (Ho and McKay, 1999) models, with their equations presented in equations (3) and (4) respectively:

$$q_t = q_e(1 - e^{-k_1 t}) \quad (3)$$

$$q_t = \frac{q_e^2.k_2.t}{1 + q_e.k_2.t} \quad (4)$$

In these models, q_t and q_e represent the sorption capacity (mg.g^{-1}) at a given time (min), and equilibrium time, respectively, while k_1 (min^{-1}) and k_2 (g.mg^{-1}.min^{-1}) are the pseudo-first order and the pseudo-second order rate constants. Moreover, to further investigate the diffusion mechanism and identify the rate-determining step, the Weber–Morris intraparticle diffusion model (Weber and Morris, 1963) was applied according to equation (5):

$$q_t = kt^{1/2} + C \quad (5)$$

where the gradient (k) is the intraparticle diffusion rate constant (mg.L^{-1}.s$^{-1/2}$) and C (mg.g^{-1}) represents the intercept related to the boundary-layer thickness.

The kinetic parameters and the correlation coefficients of pseudo–first–order, pseudo–second–order, and Weber–Morris plots are presented in Fig. 2–A, B, and Table S1. These results showed that the pseudo-first-order model yielded correlation coefficients (R^2) of approximately 0.97 for Pd, and > 0.93 for Pt and Rh (Table S1). In contrast, pseudo–second–order model demonstrated a strong fit for all three PGM, with R^2 values > 0.99 for Pd and > 96 for Pt (Table S1). The better fitting of the data in pseudo–second–order model reveals the rate–limiting step of PGM adsorption by CF is through chemisorption,

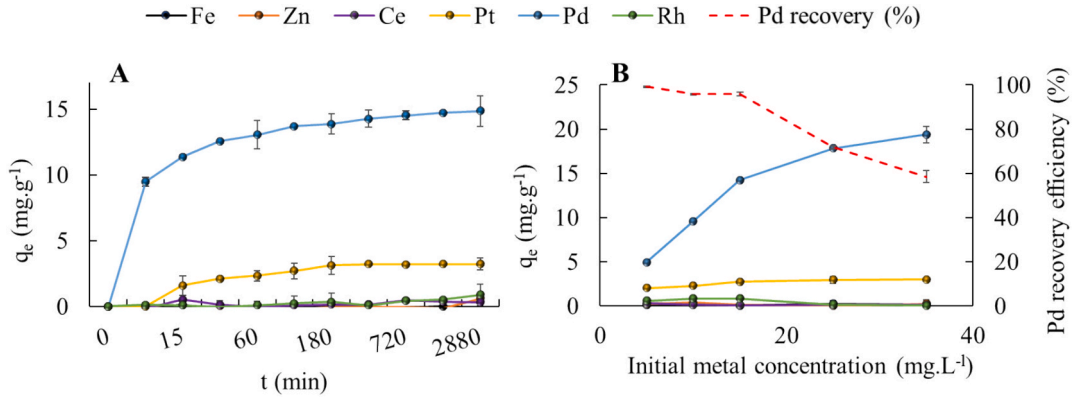

Fig. 1. (A) Adsorption kinetics of different metals by CF (initial concentrations of each metal at (15 ± 1) mg.L^{-1}) and (B) adsorption efficiency from solutions with different initial concentrations by CF (contact time of 360 min). CF dosage of 1 g.L^{-1}, HCl concentration of 0.2 M, and temperature at 303 K.

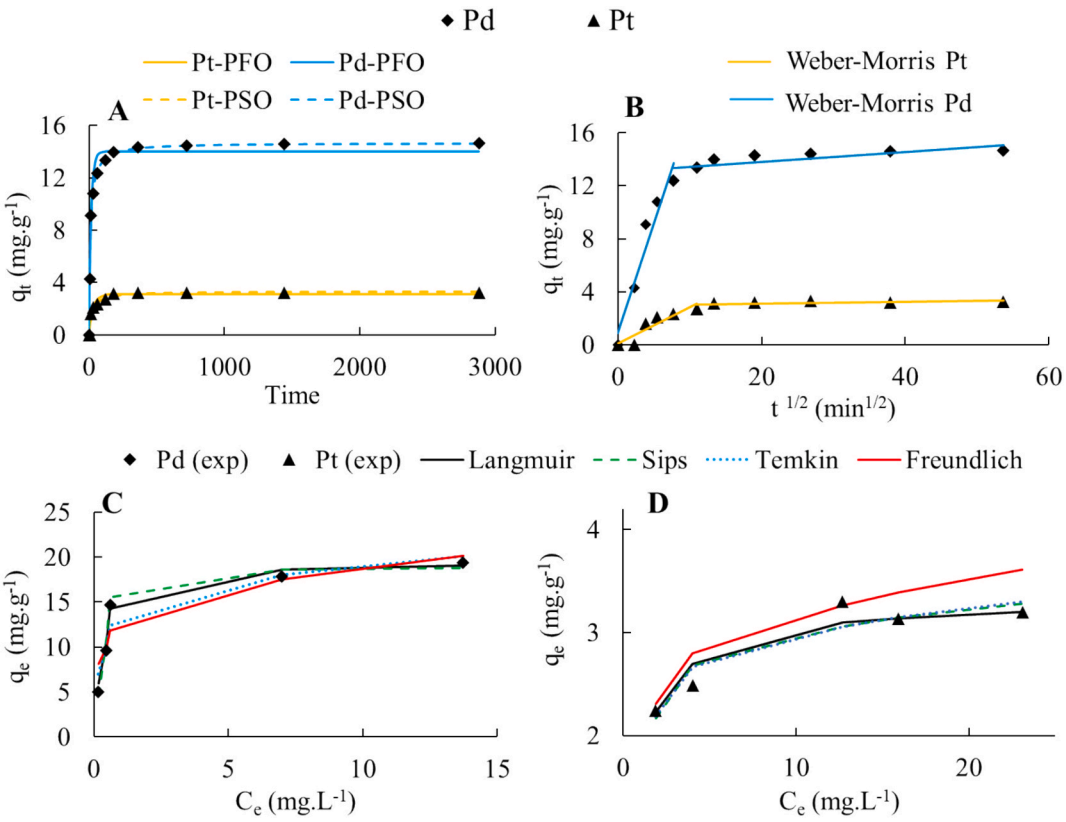

Fig. 2. (A) Nonlinear PFO and PSO kinetic fits with experimental data; (B) Weber–Morris intraparticle diffusion plots for Pd and Pt; (C–D) Nonlinear Langmuir, Freundlich, Temkin, and Sips isotherm fits for (C) Pd and (D) Pt. CF dosage of 1 $g.L^{-1}$, temperature at 303 K, and a contact time of 360 min.

involving electron sharing or exchange between sorbent and sorbate (Febrianto et al., 2009; Ho and McKay, 1999). In addition, in the pseudo–second–order model, calculated q_e values closely match experimental values for PGM ($q_{e,\ exp}$), further supporting the model's suitability (Table S1).

Furthermore, the Weber–Morris plots (Fig. 2–B) revealed two linear regions for both Pd and Pt, confirming a multi-stage diffusion process. For Pd, the steep initial segment reflects rapid film diffusion, followed by a second linear region with a lower slope, indicating continued intraparticle diffusion within the CF structure. In contrast, Pt shows only a slight increase after the initial stage, and the second region is nearly horizontal, demonstrating that intraparticle diffusion contributed minimally to its overall uptake. In both cases, the plots do not pass through the origin, showing that intraparticle diffusion was not the sole rate-limiting step. The higher diffusion constant obtained for Pd compared with Pt (Table S1) indicates a faster overall mass-transfer process, consistent with the stronger interaction and higher adsorption rate observed for Pd under identical conditions (Weber and Morris, 1963; Zamri et al., 2021).

Further experiments were performed to determine the impact of initial metal ion concentration on adsorption capacity and to estimate the maximum adsorption capacities by a fixed amount (1 $g.L^{-1}$) of adsorbent (Fig. 1–B). Results showed that the absolute amount of Pd adsorbed by CF increased with initial metal concentrations. In contrast, Pt adsorption by CF remained unaffected by changes in its initial concentration and showed a constant loading in all tests. For Rh, slight adsorption at lower concentrations (5, 10, and 15 $mg.L^{-1}$) diminished to nearly zero at 25 $mg.L^{-1}$, likely due to Pd saturating the binding sites and leaving fewer available for Rh.

Equilibrium data were analyzed using Langmuir (Langmuir, 1916), Freundlich (Freundlich, 1907), Sips (Sips, 1948), and Temkin (Temkin and Pyzhev, 1940) models (Fig. 2–C and D). Incorporation of the Temkin model, which considers adsorbate–adsorbent interactions and a linear decrease in adsorption heat, resulted in moderate fits ($R^2 = 0.94$ for Pd and 0.88 for Pt). The Temkin constants ($b_t = 6.06 \times 10^3$ for Pd and 8.47×10^2 for Pt) indicate moderate interaction energies, consistent with chemisorptive contributions for Pd (Sahmoune, 2019), but also confirming that Temkin does not describe the equilibrium behavior as accurately as the Langmuir model. Nevertheless, the Langmuir model (Equation (6) remained the only one that accurately described the equilibrium behavior for both Pd and Pt ($R^2 > 0.98$ for Pd and > 0.91 for Pt), while the other isotherms showed considerably poorer fits (Table S2).

The parameters of Langmuir model were determined using Equation (6):

$$q_e = \frac{q_{max} K_L C_e}{1 + K_L C_e} \tag{6}$$

Here q_{max} ($mg.g^{-1}$) denotes the maximum monolayer adsorption capacity, and b ($L.mg^{-1}$) is the constant associated with the adsorption bonding energy. The Langmuir isotherm model describes monolayer adsorption of solute molecules onto a uniform surface, assuming no interactions occur between the adsorbed species (Al-Ghouti and Da'ana, 2020; Langmuir, 1916). The calculated maximum adsorption capacity (q_{max}) (Table S2) using the nonlinearized form of the model was (19.61 ± 1.31) $mg.g^{-1}$ for Pd and (3.13 ± 0.18) $mg.g^{-1}$ for Pt, indicating a higher monolayer coverage capacity for Pd. Moreover, the separation factor (R_L) (Equation S2) was calculated and further assessed the adsorption feasibility, showing values for both Pd and Pt ranging from 0.03 to 0.22, confirming that the adsorption process was favorable under all tested conditions (Table S2). The data obtained for other metals, including Rh, did not fit well into the Langmuir model ($R^2 < 0.80$).

CF delivered q_{max} values often below those reported for engineered Pd adsorbents. However, two points should be considered here: (i) CFs are unmodified, waste–derived biopolymers that require no synthesis,

offering clear advantages in sustainability, cost, and scalability; benchmarking them against purpose−built materials is not one−to−one, (ii) many literature capacities are reported at modest acidity (pH 1–4), whereas our tests used 0.2 M HCl (pH ~ 0.79), a harsher, more realistic proxy for SACC leachates with roughly twice the $[H^+]/[Cl^-]$ of pH 1. The strong acidity dependence of Pd uptake is well documented, for example, thiazole−modified activated carbon shows ~30 mg·g^{-1} at pH 0, rising to ~150 mg·g^{-1} at pH 3 (Li Zhang et al., 2023a). Based on the comparative data compiled in Tables S3 and S4, CF exhibits Pd capacities lower than most engineered sorbents and industrial resins, but within the range of several bio-based adsorbents such as fungal biomass, unmodified wool (Akioka et al., 2021), terrestrial moss (Sari et al., 2009) and silica–alginate composites (Abd-Elhamid et al., 2023). A key advantage of CF is its pronounced intrinsic selectivity for Pd over Pt, Rh and cations tested, which exceeds that of many biobased sorbents and is likely linked to the high density of disulfide bridges in keratin. Relative to synthetic resins, CF still shows lower q_{max} but similar Pd selectivity. The main limitation of CF, when compared with both biobased and synthetic sorbents listed in Tables S3 and S4, is its lack of reusability.

For context (not ranking), capacities include: thiadiazole–polystyrene (176 mg·g^{-1}, 0.1 M HCl) (Zhang et al., 2022), PEI–alumina (97.7 mg·g^{-1}, pH 6) (Nagarjuna et al., 2017), ion−imprinted chitosan (36 mg·g^{-1}, 0.1 M HCl) (Baba et al., 2007), silica–alginate (12.5 mg·g^{-1}, pH 6) (Abd-Elhamid et al., 2023), Merrifield/2−benzimidazolylthioacetic acid (26 mg·g^{-1}, 0.8 M HCl) (Mahleba et al., 2025), diphenylthiophosphoryl−amide resins (53 mg·g^{-1}, 1 M HCl) (Turanov et al., 2017), Duolite GT−73 (28 mg·g^{-1}, 0.01 M HCl) (Iglesias et al., 1999), mesoporous THTB–silica (172 mg·g^{-1}, pH 3.5) (Awual et al., 2015), several with Pd stripping/reuse. Still higher values are reported for Lewatit MonoPlus TP 214 (241 mg·g^{-1}, 0.1 M HCl) (Won and Yun, 2013) and Lewatit® VP OC 1065 (290 mg·g^{-1}, 0.1 M HCl) (Wołowicz and Hubicki, 2024), though reuse was not shown. Even more extreme capacities have been reported for highly engineered dendritic sorbents, such as POSS-S-PEI, which reaches ~589 mg·g^{-1} for Pd at pH 1 but shows comparable uptake for Pt, indicating no meaningful Pd selectivity (Chaudhuri et al., 2023a). Thus, despite lower capacities relative to engineered sorbents, CF offers a sustainable and scalable route for Pd recovery, with the key advantage of maintaining functionality under the harsh acidic conditions characteristic of SACC leachates.

3.2. Effect of HCl and competing ions on PGM adsorption and selectivity

As shown in Fig. 3–A, the adsorption of metals by CF strongly depended on the HCl concentration. At 0.2 M HCl (pH 0.79 ± 0.07), Pd showed the highest adsorption (14.10 ± 0.31) mg.g^{-1}, followed by Pt (4.17 ± 0.13) mg.g^{-1}, while all other metals remained below ~1.50 mg.g^{-1}. Low Rh sorption rates, despite forming negatively charged chloride complexes, result from the bulky, poly–hydrated Rh species relative to the dehydrated anionic chloro complexes of Pd and Pt. Reducing the HCl concentration to below 0.2 M, slightly enhanced the adsorption of Rh and non–PGM, reaching ~3.00 mg.g^{-1}. On the other hand, increasing the HCl concentration to 2.0 M reduced Pd adsorption capacity to about (5.22 ± 0.16) mg.g^{-1}, while adsorption of all other metals became negligible, resulting in a relative uptake ratio (q_{Pd}/q_{Pt}) of 41.16 (Fig. 3–A). Moreover, distribution and selectivity coefficients (Tables S5) clearly reinforce these trends. At 0.2 M HCl, Pd shows a high K_d (~26.6 L.g^{-1}) and strong intrinsic selectivity, with $K_{(Pd/Pt)}$ ~75, while all other metals remain several orders of magnitude less adsorbed. At 2 M HCl, Pd capacity decreases, but selectivity remains high, with $K_{(Pd/Pt)}$ ~5 and $K_{(Pd/Rh)}$ exceeding 10^3, indicating that Pd is effectively the only metal retained under strongly acidic conditions. These results define two useful operating regimes: 0.2 M HCl for maximum Pd uptake and 2 M HCl for near-pure Pd selectivity. Moreover, according to the zeta-potential profile (Fig. S2), the CF surface remains positively charged under both 0.2 and 2 M HCl conditions. In a study by Suyama et al. (1996), the adsorption behavior of 2.5 g.L^{-1} CF from 3 mM (~320 mg.L^{-1}) monometallic Pd solutions was studied across a pH range of 1.8 to 2.2 (~15.9 mM to 6.3 mM HCl), reporting the highest adsorption at pH 2.2 with a maximum capacity of about 60 mg.g^{-1}. The present study explores a broader range of HCl concentrations, revealing a nearly constant Pd adsorption by CF across 0.04–0.2 M HCl, followed by a continuous decline as HCl concentration increases beyond this range. Moreover, Pd adsorption in this study was assessed in multimetallic systems, providing a more realistic representation of leachates where competition between metals typically reduces individual uptake compared to single−metal assays (Carreira et al., 2023). This wider operational window and the distinct adsorption profile, highlights the potential of CF in more realistic conditions, such as leachates, demonstrating their adaptability for selective PGM recovery under diverse acidic environments.

The influence of additional counter anions, including sulfate (from H_2SO_4) and nitrate (from HNO_3) on PGM adsorption by CF was examined under similar test conditions. Multimetallic solutions were prepared with a fixed HCl concentration of 0.2 M and varying concentrations of H_2SO_4 and HNO_3 (0.2, 0.5, and 1.0 M). These solutions were prepared fresh immediately before each adsorption experiment to minimize time−dependent changes in Pd speciation. For tests in H_2SO_4 and HNO_3 media, the required volume of concentrated acid was added directly to a freshly prepared Pd(II) chloride stock solution to achieve the target acid molarity. Sorption measurements were initiated immediately after mixing so that Pd remained predominantly as chloride complexes and ligand−exchange to nitrate/sulfate species during storage was avoided. As shown in Fig. 3–B and C, both H_2SO_4 and HNO_3

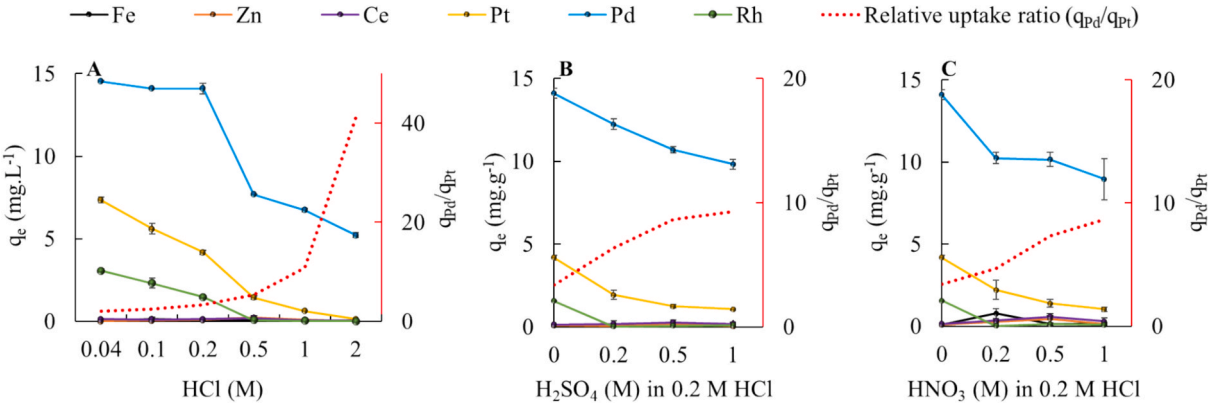

Fig. 3. Concentration influence of (A) HCl, (B) H_2SO_4 in 0.2 M HCl and (C) HNO_3 in 0.2 M HCl on the adsorption of different metals from synthetic multimetallic solutions by CF. CF dosage of 1 g.L^{-1}, initial concentrations of each metal at (15 ± 1) mg.L^{-1}, temperature at 303 K, and a contact time of 360 min.

reduced PGM adsorption compared to solutions containing only 0.2 M HCl. Among these acids, HNO_3 had a stronger inhibitory effect on PGM uptake. However, the decrease in adsorption caused by both acids was still less pronounced than the decrease observed at higher HCl concentrations. The trends in Table S5 and S6 align with this behavior, showing Pd with the highest K_d among all metals across all acids, yet its K_d decreases most sharply with increasing HCl concentration. The drop in $K_{d,Pd}$ in chloride media is substantially greater than in HNO_3 or H_2SO_4. By contrast, $K_{d,Pd}$ values in nitrate and sulfate media remain comparatively low but less sensitive to acid concentration. This is because increasing Cl^- concentration directly stabilizes soluble $[PdCl_4]^{2-}$ complexes and strongly reduces electrostatic interactions, directly suppressing the amine mediated pathway (Le Roux and Kriek, 2019). By contrast, sulfate ions mainly increase ionic strength, whereas nitrate can mildly oxidize surface sulfur groups, weakening Pd–S coordination. This suggests that an excess of chloride, nitrate, or sulfate ions compete for available adsorption sites on the adsorbent, with the greater polarizability of the chloride anion potentially facilitating surface interaction and interfering with PGM adsorption sites (Molina et al., 2011). Importantly, the results in Fig. 3 emphasize the resilience of CF as selective Pd adsorbents. In these tests, the adsorption of non–PGM remained negligible.

Furthermore, the effect of competitive metal ion concentrations on Pd adsorption by CF was evaluated by systematically increasing the concentrations of one of competitive metals (Fe, Zn, Ce, Pt or Rh) tenfold ((150 ± 5) mg.L^{-1}) while maintaining the concentration of other metals at (15 ± 1) mg.L^{-1} (Fig. S4). Results demonstrated that in all tests, Pd consistently achieved the highest adsorption levels compared to other metals. However, a measurable decline in Pd adsorption capacity was observed in tests with tenfold Pt and Rh concentrations, accompanied by an increase in their adsorption capacities (Fig. S4). This behavior is attributed to the negatively charged chloride complexes of Pt and Rh, which compete with Pd for adsorption sites on CF.

3.3. Adsorption mechanism

The presented results indicate an unexpected but obvious preference for Pd adsorption using CF over the other PGM. This selectivity is unexpected as it goes against the Hofmeister series in which greater extraction for anions of lower charge density ($[PtCl_6]^{2-}$ over $[PdCl_4]^{2-}$) is anticipated. As such, a closer evaluation of the extraction mechanism is presented.

The adsorption thermodynamics of various metals onto CFs was determined by evaluating their adsorption efficiencies at 303, 313, and 323 K (Fig. 4–A). The obtained results were used to assess the thermodynamic parameters using the van't Hoff equation (Equation S5). Fig. 4–B displays the van't Hoff's plot, illustrating the relationship between $\ln K^\circ$ and the reciprocal of temperature for Pd, Pt, and Rh, with the results summarized in Table 1. It should be noted that the thermodynamic parameters calculated via the van't Hoff equation represent apparent values under the experimental conditions used (0.2 M HCl, ~15 mg.L^{-1} metal concentration), and not standard thermodynamic values. As shown in Fig. 4–A, the adsorption of Pd increased slightly from 13.83 to 14.54 mg.g^{-1} as the temperature rose from 303 to 323 K, with a positive enthalpy suggesting an endothermic process (Table 1). This endothermic nature suggests a process that likely involves strong interactions, such as chemisorption, where bond formation between the metal ions and functional groups on the CF is favored at higher temperatures (Andrade et al., 2020; Sahmoune, 2019). The large, positive entropy change ($\Delta S = +176.68$ J·mol^{-1}·K^{-1}) further supports a mechanism involving significant structural rearrangement, contributing to the spontaneity of the process, as evidenced by increasingly negative ΔG values with rising temperature. Conversely, the same temperature increase yielded a decreased adsorption capacity of Pt from 4.76 to 4.20 mg.g^{-1}, with negative enthalpy indicating that the adsorption process for this metal is exothermic. The corresponding positive ΔG value for Pt across all tested temperatures confirms that under the studied conditions, the adsorption is non−spontaneous and thermodynamically less favorable. The moderate positive ΔS and small negative ΔH for Pt adsorption suggest weak interactions with CFs. No change in the adsorption capacities of other metals was observed.

To shed light on the thermodynamic origin of Pd selectivity by CF, Raman, solid–state UV–Vis spectroscopy, FTIR, SEM−EDX, and XPS were used to identify the functional groups present in the biomass that contribute to the adsorption of Pd. For this purpose, CF were exposed to a solution containing 100 mg.L^{-1} and 0.2 M HCl to fully saturate adsorption sites. Raman spectra of CF before and after Pd adsorption revealed the emergence of a new peak at approximately 285 cm^{-1} in the CF following Pd adsorption (Fig. 5–A). This peak corresponds to Pd–Cl stretching bonds (Clark et al., 1982), confirming that the dominant $[PdCl_4]^{2-}$ complex in the aqueous phase is maintained following the

Table 1
Apparent thermodynamic parameters under optimized experimental conditions for PGM adsorption on CF at varying temperatures.

Metal	R^2	ΔH (kJ.mol^{-1})	ΔS (J.mol^{-1}.K^{-1})	ΔG (kJ.mol^{-1}) 303 K	313 K	323 K
Pt	0.974	–8.69 ± 0.39	30.60 ± 1.46	0.60 ± 0.04	0.83 ± 0.03	1.22 ± 0.01
Pd	0.999	48.50 ± 0.89	176.68 ± 2.86	–6.47 ± 0.25	–8.17 ± 0.27	–10.00 ± 0.29
Rh	0.992	–23.49 ± 0.15	–103.22 ± 6.58	7.74 ± 0.87	8.89 ± 0.91	9.80 ± 0.96

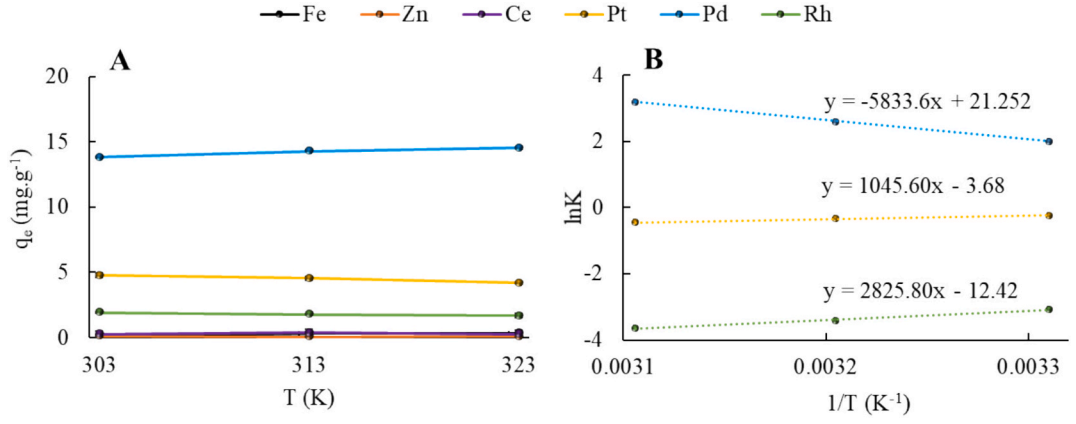

Fig. 4. (A) Effect of temperature on adsorption efficiency of tested metals and (B) van't Hoff plot for thermodynamic analysis of PGM adsorption by CF. CF dosage of 1 g.L^{-1}, HCl concentration of 0.2 M, initial concentrations of each metal at (15 ± 1) mg.L^{-1} and a contact time of 360 min.

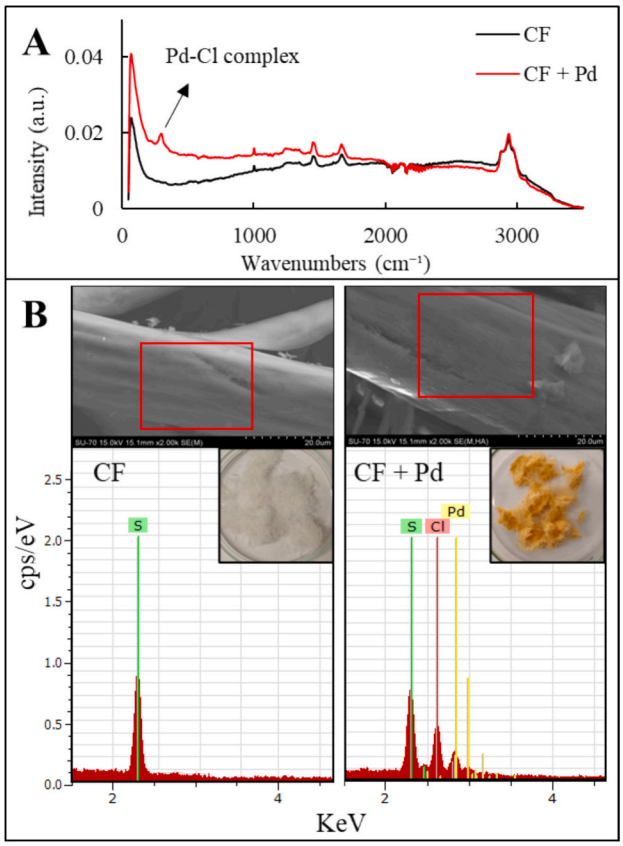

Fig. 5. (A) Raman spectra and (B) SEM–EDX mapping of CF before and after Pd adsorption from a 100 mg/L Pd solution in 0.2 M HCl. CF dosage of 1 $g.L^{-1}$, temperature at 303 K, and a contact time of 360 min.

adsorption process. Such a conclusion is visually supported by the orange coloring of the CF post adsorption, characteristic of $[PdCl_4]^{2-}$ anions. Solid–state UV–Vis spectra (Fig. S5) of CF post−adsorption displays a new band at 389 nm, consistent with ligand–to–metal charge transfer (Lever, 1974) as observed in $[PdCl_4]^{2-}$ complexes. Regarding FTIR analysis, no significant spectral changes were observed in the functional groups before and after Pd adsorption (Fig. S6), likely due to its relatively low adsorption capacity (~19.61 $mg.g^{-1}$; Table S2).

SEM images of CF before and after Pd adsorption (Fig. S7) further confirm this, with CF following Pd adsorption exhibiting well–defined Pd and Cl peaks not observable prior to adsorption (Fig. 5–B). The elemental compositions of untreated and Pd–adsorbed CF analyzed by SEM–EDX are summarized in Table S7 and indicate an approximate Cl: Pd ratio of 3.38, consistent with the presence of anionic Pd–chloro complexes. Moreover, the absence of localized Pd−rich spots after Pd adsorption indicates that Pd is homogeneously adsorbed over the fibers rather than forming nanoparticles (Fig. 5–B; Fig. S7 and S8).

XPS analysis of the surface elemental composition is summarized in Table S8 and further supports the SEM and Raman conclusions. As shown, the Cl/Pd atomic ratio is notably high, approximately 4.76, which suggests that Pd was primarily adsorbed in the form of Cl–Pd complexes and/or that residual chloride ions remain associated with the surface after adsorption. From these results, speciation changes do not appear to be the determining factor for Pd selectivity over Pt.

XPS spectra of CF were examined before and after Pd adsorption (Fig. 6), with corresponding binding energies and atomic percentages provided in Table S9. Special attention was paid to the N and S binding energies of the adsorbent keratin protein. In the survey spectra, a new signal appears in the 337.8– 343.1 eV range after Pd adsorption, consistent with the Pd^{2+} oxidation state. Notably, no peaks corresponding to metallic Pd^0 were detected. The high–resolution S 2p spectra reveal a notable shift in the relative intensities of S species. In untreated CF (Fig. 6–C), dominant peaks at ~163.8 eV (S $2p_{3/2}$) are attributed to disulfide and thiol groups, while a secondary peak at ~167.6 eV corresponds to oxidized sulfur species such as sulfonates or sulfates. After Pd adsorption (Fig. 6–C), the intensity of the 163.8 eV peak decreases, while the oxidized sulfur contribution increases. This suggests that sulfur–containing functionalities, particularly disulfide bridges and thiols participate in Pd coordination, likely via Pd–S coordination. In line with Petrov (2023), in HCl media $[PdCl_4]^{2-}$ can interact with disulfide (–S–S–) linkages in two ways: (i) coordination to the intact disulfide, where polarization of the S–S bond weakens it without full cleavage, and (ii) partial scission of the disulfide, yielding –SH groups that coordinate to Pd. In the feather matrix, these perturbed sulfur sites undergo further aerobic oxidation into $S–O_x$ species (sulfenic/sulfinic/sulfonic), which is consistent with the observed decrease of the disulfide/thiol contribution and the corresponding increase of oxidized−S signals in XPS. Changes in the high–resolution N 1s spectra further support the involvement of N functionalities (Fig. 6–D). Prior to Pd exposure, the N 1 s region displays peaks at ~399.2 eV (C–N/peptide), 400.5 eV (amide/neutral amine), 401.9 eV (protonated amine/amide), and 403.0 eV. After Pd uptake, the protonated/oxidized contributions diminish (at ~401.9 eV and ~403–403.5 eV), while the neutral amide/amine increases (peak at ~400.5 eV), with a small growth of the ~399.2 eV shoulder. No new N 1s component appears. These changes indicate partial deprotonation/disruption of $–NH_3^+$ ion pairs and local rearrangement of the peptide/amine environment upon association of $[PdCl_4]^{2-}$ near cationic sites, consistent with electrostatic outer−sphere ion pairing rather than strong Pd–N chelation under the acidic conditions used (Nikoloski et al., 2015; Wołowicz and Hubicki, 2012).

To better discriminate the respective contributions of amine and disulfide groups in Pd adsorption onto CF, two targeted experiments were conducted. To reveal the role of amine groups, a solution containing (15 ± 1) $mg.L^{-1}$ of Pd was prepared, and its pH was adjusted to 5, slightly above the isoelectric point of keratin (pH 4.4). To prevent decomplexation and hydrolysis of Pd–Cl complexes, NaCl was added to achieve a final concentration of 0.1 M. Subsequently, CF were introduced at a concentration of 1 $g.L^{-1}$. At this pH, amino groups are expected to be largely deprotonated and, therefore, not electrostatically involved in Pd adsorption. The adsorption capacity was found to be (9.04 ± 0.2) $mg.g^{-1}$, representing a ~25% reduction compared to that observed at 0.2 M HCl without pH adjustment (Fig. S9). This suggests that amine groups are not the sole functional groups involved in Pd adsorption. To assess the contribution of disulfide bonds in Pd adsorption, CF underwent a targeted chemical modification process to chemically attack and remove the disulfide bond (see SI Section 1.3 of the Experimental section). The modified material was precipitated, and circular dichroism (CD) analysis confirmed the loss of secondary structure and increased disorder post–cleavage and capping (Fig. S10), confirming the successful cleavage and capping of the S–S bonds. The modified CF were then tested in a (15 ± 1) $mg.L^{-1}$ Pd solution containing 0.2 M HCl. These treated CF exhibited a significantly reduced Pd adsorption capacity of (6.4 ± 0.1) $mg.g^{-1}$, a ~60% decrease compared to untreated CF, highlighting the critical role of disulfide bonds and thiol groups in Pd adsorption (Fig. S9). This is also evident in Fig. 3−A, where increasing HCl from 0.2 to 0.5 M sharply compresses the electrical double layer (higher ionic strength) and raises Cl^- activity, which together quench the amine−mediated electrostatic pathway (screening + site occupation), causing the abrupt drop in capacity. Beyond ~0.5 M, adsorption is dominated by the S−coordination pathway, which is far less sensitive to ionic strength, so further increases to 1–2 M lead only to modest additional decreases. This behavior aligns with observations that ionic strength can suppress electrostatic adsorption mechanisms (Sebben and Pendleton, 2015) and that anions can compete with metal ion uptake at amine sites, shifting uptake to other functional groups (Weißpflog et al., 2020). This trend also agrees with the adsorption kinetics (Fig. 1−A), which exhibit a rapid initial uptake of Pd followed by

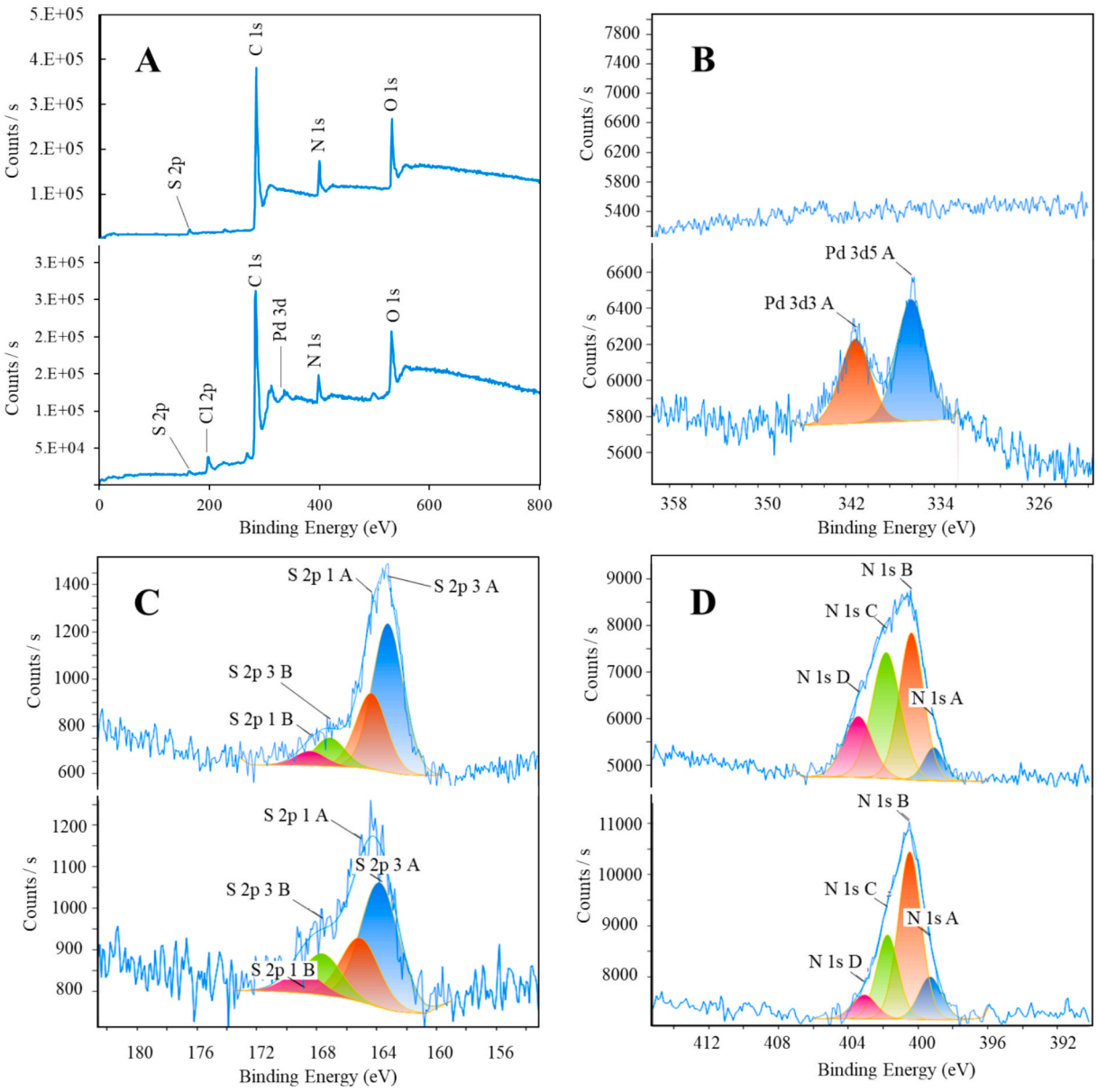

Fig. 6. (A) Wide–scan XPS survey spectra. High–resolution XPS spectra of (B) Pd 3d, (C) S 2p, and (D) N 1 s regions. Each panel shows spectra of CF before (top) and after Pd adsorption (bottom).

a slower approach to equilibrium. The fast stage can be attributed to interactions with readily accessible surface amino groups, while the slower, rate−limiting phase involves the interaction of $[PdCl_4]^{2-}$ with disulfide linkages. In this step, $[PdCl_4]^{2-}$ polarizes and weakens the S–S bonds, leading either to coordination as S,S−binuclear Pd–disulfide complexes or to partial cleavage of disulfides, with the resulting thiol/thiolate species binding Pd (Petrov, 2023). Diffusion of $[PdCl_4]^{2-}$ into the keratin matrix may also contribute to a second rate−limiting factor (Paul et al., 2023).

In light of the mechanistic results presented, a schematic of the potential extraction mechanisms is presented in Fig. 7. Adsorption between the anhydrous anionic complexes and the protonated amino groups originating from side–chain amino acids on keratin in HCl matrix is expected to contribute approximately 40% of the Pd uptake capacity. This extraction mechanism does not discriminate between PGM (Pt *vs* Pd) and decreases with acid concentration, attributable to competition between Cl^- ions and the negatively charged Pd–chloride complexes for binding sites on the CF surface (Fig. 7). Approximately 60% of the $[PdCl_4]^{2-}$ adsorption capacity is attributed to disulfide bonds naturally present in keratin, which arise from the oxidation of cysteine residues forming covalent S–S linkages. As described by Petrov (2024, 2023) and Luo et al (1999), $[PdCl_4]^{2-}$ can form robust S,S–binuclear complexes $[Pd_2Cl_x(R–SS–R)]$, which remain stable even in elevated Cl^- environments. Pd coordination to one sulfur atom can also weaken the disulfide bond, allowing nucleophilic attack by water or chloride ions, which cleaves the bond. This cleavage yields thiol–containing species (R–SH), which subsequently coordinate with Pd to form stable $[PdCl_x(R–S)]$ complexes (Luo et al., 1999; Petrov, 2024, 2023). In either case, Pd's "soft" character promotes strong Pd–S bonding, allowing it to interact with disulfide groups both through direct bridging and via bond cleavage followed by thiol coordination. Through this pathway, the planar organization of the $[PdCl_4]^{2-}$ complex relative to the octahedral geometry $[PtCl_6]^{2-}$ facilitates this interaction and gives rise to the observed adsorption preference using CF. However, the precise structure of the resulting Pd species on the CF surface remains undetermined. It is plausible that one or more Cl^- ligands are displaced during Pd–S complexation, potentially forming mixed–ligand species. This dual mechanism, in which amine and disulfide bonds are involved,

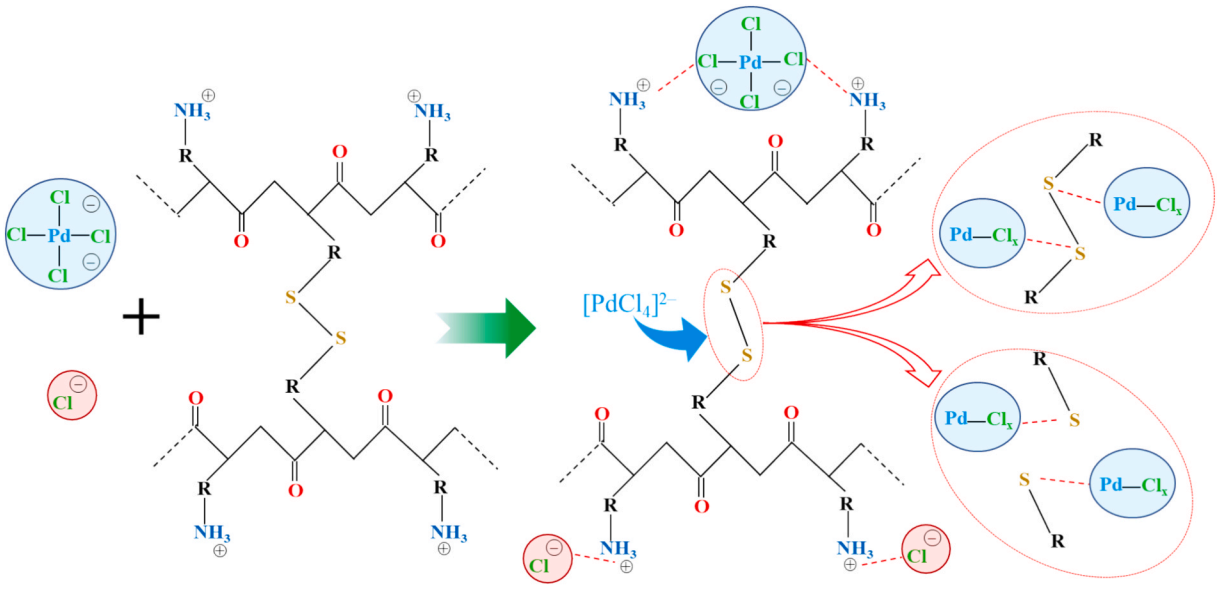

Fig. 7. Suggested mechanism of Pd adsorption by CF in an HCl matrix. The keratin polypeptide backbone, with protonated amino groups from side–chain amino acids such as lysine and arginine (Maurya and Singh, 2023), interacts with $[PdCl_4]^{2-}$ and Cl^- ions.

contributes to the overall Pd adsorption by CF.

3.4. Desorption

CF with adsorbed metals, obtained at optimized conditions from tests with synthetic solutions were subjected to desorption using different agents including HCl, NaOH, and acidified thiourea (Fig. S11). Comprehensive desorption studies, including experimental conditions and recovery efficiencies, are presented in the Supporting Information (SI Section 2.7). Results showed that HCl effectively desorbs Pt, leaving Pd more selectively retained on CF, while 0.2 M thiourea + 0.5 M HCl enabled nearly complete Pd desorption (Fig. S11). These two steps can be applied sequentially to enhance the separation and purification of Pt and Pd.

3.5. Application to real leachates

After conducting evaluations with synthetic solutions and optimizing various parameters, the obtained data provided valuable insights for refining the conditions to maximize Pd recovery from real leachates. Therefore, tests were performed to evaluate the applicability of the obtained parameters to real leachates from SACC. Metal concentrations were measured in the original leachates from both MixC and VW90 (with ~12 M HCl), as well as in their 6−and 60−fold dilutions (corresponding to final HCl concentrations of 2.0 and 0.2 M, respectively) (Table S11). These dilution levels were chosen based on prior findings: 0.2 M HCl yielded the highest Pd adsorption capacity with lower co–adsorption of other metals, while 2.0 M HCl demonstrated the greatest selectivity for Pd adsorption (Fig. 3–A).

Metal adsorption tests with the 60-fold diluted leachates confirmed that Pd was the only metal significantly adsorbed, as shown in Fig. S13 and described in detail in Section 2.10 of the SI. For the 6-fold diluted leachates, successive adsorption cycles were carried out using 5 $g.L^{-1}$ of fresh CFs, based on the adjusted maximum adsorption capacity ($q_{max,\ adjusted}$ = 6.47 $mg.g^{-1}$; Section 2.10, SI). In the VW90 leachate, Pd removal progressively decreased to below detection limits after five adsorption cycles (Fig. 8 and Table S12). Pd selectivity remained high, with minimal co-adsorption of Pt, Rh, or other metals. Similar performance was observed for the diluted MixC leachate, and three adsorption cycles were found to be enough to reduce Pd levels below the limit of detection. The optimization steps (Section 2.10, SI), together with the cumulative adsorption profiles (Fig. 8 Table S12), confirm that extraction trends and Pd selectivity across acid concentrations in real leachates are consistent with those obtained from synthetic mixtures.

The exceptional selectivity of CF toward Pd in both leachates demonstrates its strong potential for real−world leachate treatment applications. To further assess this feasibility, single−step adsorption and desorption tests were performed using the MixC leachate, which serves as a more realistic representation due to the greater relative concentrations of competing ions (Table S11). To improve the selectivity towards Pd whilst reducing the total volume of leach solution to treat, Pd recovery from 1/6 diluted MixC leachate was assessed, involving a single–step Pd adsorption followed by a selective Pt separation and finally, complete desorption of Pd from CF. Based on prior results with MixC leachate (see Fig. 8), which demonstrated two adsorption cycles with 5 $g.L^{-1}$ of CF were sufficient to adsorb over 97% of Pd, a single–step adsorption process was tested using 10 $g.L^{-1}$ of CF. Moreover, Pt separation step was designed based on findings from desorption studies with HCl (Fig. S11), which showed 0.5 M HCl can selectively desorb nearly 70% of Pt from CF, thus leaving Pd in a purer state. Results, summarized in Fig. 9 demonstrate that approximately 95% of Pd, equivalent to ~7.3 $mg.g^{-1}$ CF, was successfully recovered from the leachate. In contrast, only around 25% of Pt (~1.2 $mg.g^{-1}$ CF) was adsorbed, with no detectable adsorption of Rh or other metals. No significant changes were observed in the concentrations of other metals throughout this study, this includes metals tested in optimization steps (Fe, Zn and Ce) and also other metals present in the leachate including Ti, Ni and Cu. To enhance the purity of the adsorbed Pd on CF, a scrubbing step with 0.5 M HCl effectively removed approximately 70% of the adsorbed Pt, reducing Pt content on the CF from ~1.2 $mg.g^{-1}$ to ~0.36 $mg.g^{-1}$ CF, while minimizing Pd co–desorption (~5%, accounting for ~0.37 $mg.g^{-1}$ CF) (Fig. 9). In the final step, CF were treated with a desorption solution of 0.2 M TU + 0.5 M HCl (10 $g.L^{-1}$ of CF), achieving nearly 100% desorption of both Pd and the remaining Pt. This multi–step process validated the efficiency of the approach for the selective recovery and purification of PGM.

In an identical study, after the desorption step, CF were thoroughly rinsed with distilled water, dried, and reused for second and third adsorption–desorption cycles. However, a substantial decrease in adsorption efficiency was observed in these subsequent cycles. To ascertain whether this decline arose from the HCl in the leachate or from the TU desorption solution, CF were exposed to 2 M HCl; half were then

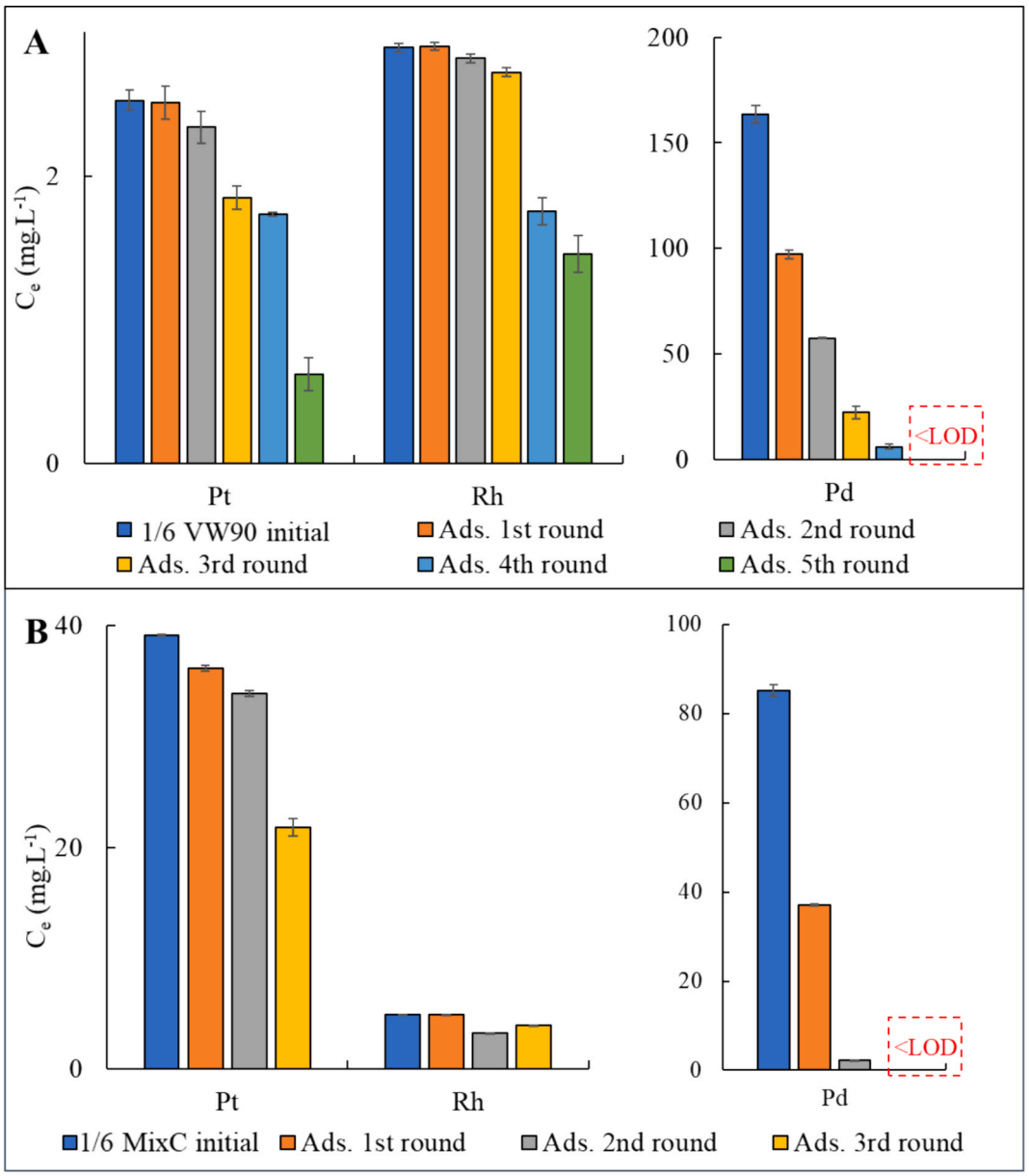

Fig. 8. PGM concentration on 1/6 diluted leachates after contact with CF: (A) VW90 and (B) MixC. CF dosage of 5 g.L^{-1} in each cycle, temperature at 303 K, and a contact time of 360 min.

removed for sampling, and the remainder was further treated with 0.2 M TU + 0.5 M HCl. Both CF subsets were subsequently tested for metal adsorption from the 1/6 diluted MixC leachate with 10 g.L^{-1} of CF. Results showed that CF exposed only to 2 M HCl retained adsorption performance comparable to untreated CF, whereas those subjected to the TU–containing solution exhibited a markedly reduced Pd adsorption capacity (Fig. S14). These findings suggest that thiourea may chemically interact with and modify the CF surface, impairing its metal–binding functionality. This is consistent with the previous CD and XPS results, which confirmed significant denaturation of the keratin three−dimensional structure due to the breaking of the disulfide backbone during Pd desorption by thiourea, hindering its reusability (Fig. S12). Consequently, CF lose nearly 50% of their adsorption efficiency after one adsorption–desorption cycle (Fig. S14). While further optimization of the desorption step could mitigate this issue, considering the negligible cost and high availability of CF as a waste material, a more practical strategy may involve a single adsorption followed by TU desorption, after which the spent CF can be discarded.

Another potential approach is to convert metal–loaded CF into Pd–containing activated carbon. As TGA analysis showed (Fig. S15), both untreated and Pd–adsorbed CF leave a significant carbon–rich residue above 800 °C, suitable for producing activated carbon. This strategy not only simplifies the recovery process through elimination of the desorption step, but also adds value by producing a material with significant catalytic potential. The resulting activated carbon benefits from the inherent properties of activated carbon, such as high surface area and chemical inertness, while the presence of Pd and Pt imparts unique catalytic functionalities relevant to a number of applications.

3.6. *Scaling keratinous wastes as a renewable sorption reservoir*

From a circular-economy perspective, the present work is best framed as a waste-to-waste valorization route based on keratin-rich CF. CF form a globally abundant keratin stream generated at about 10 million tons each year as an inherent output of poultry processing, with both consistent supply and worldwide distribution (FAO, 2023;

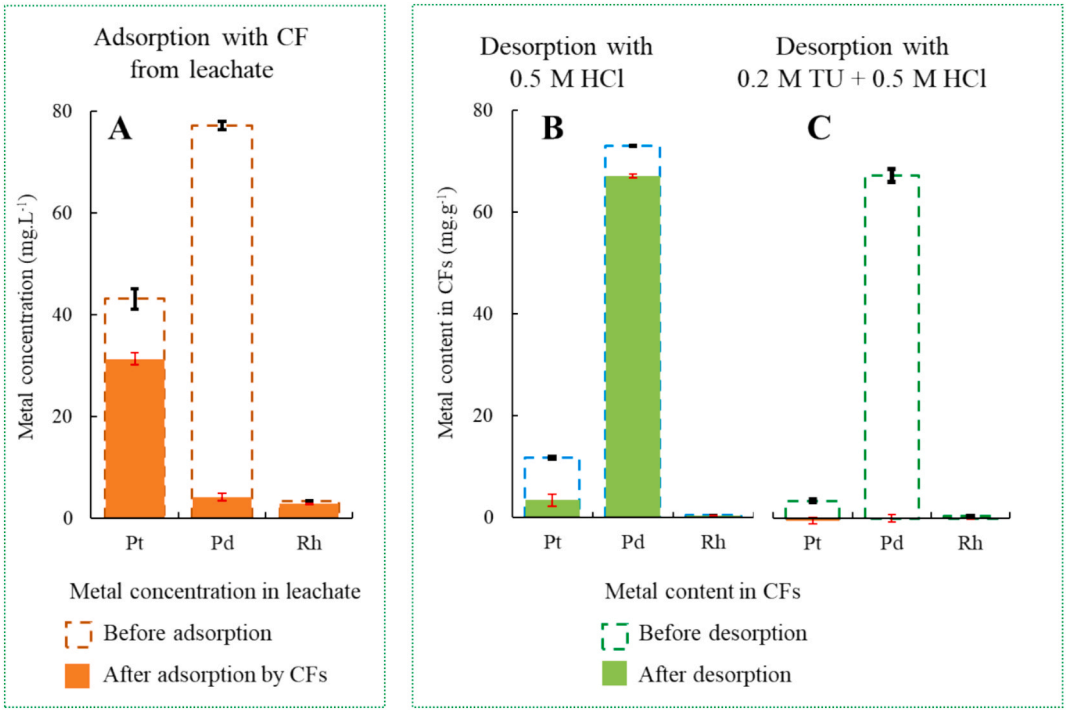

Fig. 9. (A) PGM adsorption from 1/6 diluted MixC leachate by 10 $g.L^{-1}$ of CF and (B) Pt desorption from CF using 0.5 M HCl, followed by (C) Pd and Pt desorption by 0.2 M TU + 0.5 M HCl. CF dosage of 10 $g.L^{-1}$, temperature at 303 K, and a contact time of 360 min.

Grazziotin et al., 2006; Long Zhang et al., 2023). Taking the experimentally obtained results, CF show Pd uptakes of ~14 $mg.g^{-1}$ at 0.2 M HCl (maximum capacity) and ~5 $mg.g^{-1}$ at 2 M HCl (maximum selectivity). This behavior is fully reflected in real SACC leachates. In 1/60 diluted leachates (0.2 M HCl), CF reach ~10–14 $mg.g^{-1}$, achieving nearly complete Pd removal at 1 $g.L^{-1}$ CF. On the other hand, 1/6 diluted leachates (~82 $mg.L^{-1}$ Pd, 2 M HCl) show lower intrinsic capacity but far higher selectivity: using 10 $g.L^{-1}$ CF, all Pd is removed in a single adsorption step, corresponding to an effective uptake of ~8.2 $mg.g^{-1}$ under harsh acidic conditions. These experimentally validated ranges correspond to a practical Pd-capture potential of 5–14 kg Pd per ton of CF, depending on acidity and feed composition. Reported Pd contents in SACC range from ~0.1–0.8 g per unit in lower-loaded catalysts up to ~1–2 g per unit in typical gasoline SACC, with an average of ~1.6 g Pd per SACC often cited (Nobahar et al., 2023; Vasile et al., 2021; Yakoumis et al., 2018; Yousif, 2019). Based on these values, 1 ton of CF at q_e ~14 $mg.g^{-1}$ provides sufficient sorption capacity to capture the Pd contained in approximately 3000 to 70 000 SACC, depending on catalyst grade.

Extending these mass-balance considerations to the broader global keratin stream, including human hair, wool, animal bristles, hooves, and mixed slaughterhouse byproducts, collectively contributes over 12 million tons of keratin-containing material each year, sharing comparable amine and disulfide-rich protein structures capable of metal coordination (Banasaz and Ferraro, 2024; Mattiello et al., 2022). Scaling the same uptake values from CF to this broader keratin stream proportionally expands the theoretical sorption reservoir, demonstrating that keratinous wastes as a whole constitute a large, renewable, and underutilized resource for circular metal-recovery technologies. These mass-balance considerations establish a quantitative and scalable foundation for the circular-economy motivation of this work while remaining fully aligned with its chemistry-focused scope and without requiring keratin extraction or synthetic modification of the feathers.

4. Conclusions

This study presents an innovative and sustainable approach for Pd recovery from spent catalytic converter leachates using CF, a widely available keratin–rich waste material. A comprehensive experimental framework combining batch adsorption experiments with validation in real HCl-based leachates were used to assess the feasibility of CF as a Pd-selective sorbent under realistic hydrometallurgical conditions.

Adsorption experiments with synthetic multimetallic solutions demonstrated a pronounced selectivity of CF toward Pd, with Langmuir maximum capacity of (19.61 ± 1.31) $mg.g^{-1}$, while Pt adsorption remained limited ((3.13 ± 0.18) $mg.g^{-1}$) and Rh and non-PGM were negligibly adsorbed. Increasing the HCl concentration to 2 M reduced Pd capacity but maximized selectivity, yielding q_{Pd}/q_{Pt} ratios above 40, thereby defining two practical operating regimes for maximum Pd uptake or near-pure Pd separation. Kinetic and equilibrium data were best described by the pseudo-second-order model and the Langmuir isotherm, respectively, indicating chemisorption on energetically homogeneous sites. Efficient Pd desorption was achieved using acidified thiourea solution, although CF reusability was compromised.

Thermodynamic analysis confirmed endothermic and spontaneous Pd adsorption, in contrast to non-spontaneous Pt uptake. Spectroscopic and microscopic analyses showed that Pd is retained predominantly as chloride complexes interacting with keratin disulfide bonds, with secondary contributions from protonated amino groups. Targeted chemical modification experiments confirmed that approximately 60% of Pd uptake originates from disulfide-mediated coordination, explaining the persistence of Pd adsorption at high chloride concentrations.

Finally, application to real spent catalytic converter leachates validated the robustness of the process. Near-complete Pd recovery was achieved from 1/60 and 1/6 diluted leachates in a single step using 1 and 10 $g.L^{-1}$ CF, respectively, while sequential adsorption–desorption enabled ~95% Pd recovery with minimal co-adsorption of Pt or other metals.

Their renewable origin, biodegradability, and the absence of any synthetic preparation steps make CF a valuable green alternative for Pd

recovery, particularly when economic and environmental considerations are prioritized over maximum efficiency. By coupling adsorption and desorption performance, mechanistic insights and validation in real leachates under harsh acidic conditions, this study establishes CF as a viable waste-to-waste sorbent for selective Pd isolation and extends the applicability of keratin-based materials beyond idealized laboratory systems.

Declaration of generative AI in writing

During the preparation of this work the author(s) used ChatGPT in order to improve grammar and clarity. After using this tool/service, the author(s) reviewed and edited the content as needed and take(s) full responsibility for the content of the published article.

CRediT authorship contribution statement

Amir Nobahar: Writing – original draft, Validation, Methodology, Investigation, Formal analysis. **Flavia N. Braga:** Writing – review & editing, Investigation, Formal analysis. **Filipe H.B. Sosa:** Writing – review & editing, Supervision, Funding acquisition. **Nicolas Schaeffer:** Writing – review & editing, Supervision, Methodology, Conceptualization. **João A.P. Coutinho:** Writing – review & editing, Supervision, Resources, Conceptualization. **Helena Passos:** Writing – review & editing, Supervision, Resources, Funding acquisition, Conceptualization.

Declaration of competing interest

The authors declare that they have no known competing financial interests or personal relationships that could have appeared to influence the work reported in this paper.

Acknowledgments

This work was financially supported by national funds through FCT – Fundação para a Ciência e a Tecnologia, I.P., within the scope of the project PlatILPlus (2022.04478.PTDC, DOI: 10.54499/2022.04478.PTDC). This work was further financially supported by Fundação para a Ciência e a Tecnologia, I.P. /MCTES through national funds: LSRE-LCM, UID/50020/2025 (DOI: 10.54499/UID/50020/2025); ALiCE, LA/P/0045/2020 (DOI: 10.54499/LA/P/0045/2020); and CICECO-Aveiro Institute of Materials, UID/50011/2025 (DOI: 10.54499/UID/50011/2025) & LA/P/0006/2020 (DOI 10.54499/LA/P/0006/2020). N. Schaeffer acknowledges the European Research Council (ERC) for the starting grant ERC–2023–StG–101116461. F.H.B. Sosa and F. Braga acknowledge FCT for the researcher contract CEECIND/07209/2022 (10.54499/2022.07209.CEECIND/CP1720/CT0019) and the Ph.D. grant 2023.01749.BD (DOI:10.54499/2023.01749.BD), respectively. The authors also acknowledge Valorcar – Sociedade de Gestão de Veículos em fim de Vida Lda. for providing the spent automotive catalytic converters.

Appendix A. Supplementary data

Supplementary data to this article can be found online at https://doi.org/10.1016/j.wasman.2026.115349.

Data availability

Data will be made available on request.

References

Abd-Elhamid, A.I., Abu Elgoud, E.M., Aly, H.F., 2023. Adsorption of palladium from chloride aqueous solution using silica alginate nanomaterial. Int. J. Biol. Macromol. 253, 126754. https://doi.org/10.1016/j.ijbiomac.2023.126754.

Akioka, S., Hirai, S., Ise, T., Gando, N., Alharbi, M.A.H., 2021. Selective recovery of palladium by wool resin and woven wool fabric resinrbents. Hydrometall. 203, 105629. https://doi.org/10.1016/j.hydromet.2021.105629.

Al-Ghouti, M.A., Da'ana, D.A., 2020. Guidelines for the use and interpretation of adsorption isotherm models: A review. J. Hazard. Mater. 393, 122383. https://doi.org/10.1016/j.jhazmat.2020.122383.

Andrade, C.A., Zambrano-Intriago, L.A., Oliveira, N.S., Vieira, J.S., Quiroz-Fernández, L. S., Rodríguez-Díaz, J.M., 2020. Adsorption behavior and mechanism of oxytetracycline on rice husk ash: Kinetics, equilibrium, and thermodynamics of the process. Water Air Soil Pollut. 231, 103. https://doi.org/10.1007/s11270-020-04473-6.

Awual, M.R., Hasan, M.M., Naushad, Mu., Shiwaku, H., Yaita, T., 2015. Preparation of new class composite adsorbent for enhanced palladium(II) detection and recovery. Sens. Actuators B Chem. 209, 790–797. https://doi.org/10.1016/j.snb.2014.12.053.

Baba, Y., Ohe, K., Ohshima, T., Dhakal, R.P., 2007. Preparation of palladium(II)-imprinted chitosan derivative and its adsorption properties of precious metals. J. Ion Exch. 18, 226–231. https://doi.org/10.5182/jaie.18.226.

Banasaz, S., Ferraro, V., 2024. Keratin from animal by-products: Structure, characterization, extraction and application—A review. Polymers 16, 1999. https://doi.org/10.3390/polym16141999.

Bongers, J., Richardson, D.E., Bell, J.U., 1988. Platinum(II) binding to metallothioneins. J. Inorg. Biochem. 34, 55–62. https://doi.org/10.1016/0162-0134(88)85017-7.

Carreira, A.R.F., Schaeffer, N., Passos, H., Coutinho, J.A.P., 2023. Sorption as a pre-concentration step for metal ions recovery in multi-elemental systems. Chem. Eng. Res. Des. 192, 546–555. https://doi.org/10.1016/j.cherd.2023.03.013.

Chakraborty, R., Asthana, A., Singh, A.K., Yadav, S., Susan, M.A.B.H., Carabineiro, S.A. C., 2020. Intensified elimination of aqueous heavy metal ions using chicken feathers chemically modified by a batch method. J. Mol. Liq. 312, 113475. https://doi.org/10.1016/j.molliq.2020.113475.

Chaudhuri, H., Dash, S., Sarkar, A., 2016. Fabrication of new synthetic routes for functionalized Si-MCM-41 materials as effective adsorbents for water remediation. Ind. Eng. Chem. Res. 55, 10084–10094. https://doi.org/10.1021/acs.iecr.6b02241.

Chaudhuri, H., Lim, C.-R., Yun, Y.-S., 2023a. Polyethylenimine functionalized sulfur-containing POSS-based dendritic adsorbent for highly efficient and selective capturing of precious metal ions. Desalination 566, 116925. https://doi.org/10.1016/j.desal.2023.116925.

Chaudhuri, H., Lin, X., Yun, Y.-S., 2023b. Graphene oxide-based dendritic adsorbent for the excellent capturing of platinum group elements. J. Hazard. Mater. 451, 131206. https://doi.org/10.1016/j.jhazmat.2023.131206.

Chen, H., Yang, X., Liu, Y., Lin, X., Wang, J., Zhang, Z., Li, N., Li, Y., Zhang, Y., 2021. KOH modification effectively enhances the Cd and Pb adsorption performance of N-enriched biochar derived from waste chicken feathers. Waste Manag. 130, 82–92. https://doi.org/10.1016/j.wasman.2021.05.015.

Chen, Z., Chen, Y., Xu, T., Guo, Y., He, T., Xie, H., Zhang, L., 2025. Upcycling of wool keratin for selective recovery of gold from aqueous solution. Chem. Eng. J. 503, 158324. https://doi.org/10.1016/j.cej.2024.158324.

Clark, R.J.H., Kurmoo, M., Mountney, D.N., Toftlund, H., 1982. Electronic and resonance Raman spectra of mixed-valence, linear-chain complexes of platinum and palladium with 1,2-diaminocycloalkanes (N–N), [MII (N–N)2][MIV (N–N)2 X2]X4 (X = halogen). J. Chem. Soc. Dalton Trans. 1851–1860. https://doi.org/10.1039/DT9820001851.

Dhaouadi, F., Sellaoui, L., Badawi, M., Reynel-Ávila, H.E., Mendoza-Castillo, D.I., Jaime-Leal, J.E., Bonilla-Petriciolet, A., Lamine, A.B., 2020. Statistical physics interpretation of the adsorption mechanism of Pb2+, Cd2+ and Ni2+ on chicken feathers. J. Mol. Liq. 319, 114168. https://doi.org/10.1016/j.molliq.2020.114168.

Enkhzaya, S., Shiomori, K., Oyuntsetseg, B., 2020. Effective adsorption of Au(III) and Cu (II) by chemically treated sheep wool and the binding mechanism. J. Environ. Chem. Eng. 8, 104021. https://doi.org/10.1016/j.jece.2020.104021.

FAO, F. and A.O. of the U.N., 2023. Meat market review: Emerging trends and outlook 2023.

Febrianto, J., Kosasih, A.N., Sunarso, J., Ju, Y.-H., Indraswati, N., Ismadji, S., 2009. Equilibrium and kinetic studies in adsorption of heavy metals using biosorbent: A summary of recent studies. J. Hazard. Mater. 162, 616–645. https://doi.org/10.1016/j.jhazmat.2008.06.042.

Freundlich, H., 1907. Über die Adsorption in Lösungen. Z. Für Phys. Chem. 57U, 385–470. https://doi.org/10.1515/zpch-1907-5723.

Grazziotin, A., Pimentel, F.A., De Jong, E.V., Brandelli, A., 2006. Nutritional improvement of feather protein by treatment with microbial keratinase. Anim. Feed Sci. Technol. 126, 135–144. https://doi.org/10.1016/j.anifeedsci.2005.06.002.

Grilli, M.L., Slobozeanu, A.E., Larosa, C., Paneva, D., Yakoumis, I., Cherkezova-Zheleva, Z., 2023. Platinum group metals: Green recovery from spent auto-catalysts and reuse in new catalysts—A review. Crystals 13, 550. https://doi.org/10.3390/cryst13040550.

Ho, Y.S., McKay, G., 1999. Pseudo-second order model for sorption processes. Process Biochem. 34, 451–465. https://doi.org/10.1016/S0032-9592(98)00112-5.

Iglesias, M., Anticó, E., Salvadó, V., 1999. Recovery of palladium(II) and gold(III) from diluted liquors using the resin duolite GT-73. Anal. Chim. Acta 381, 61–67. https://doi.org/10.1016/s0003-2670(98)00707-7.

Il Yoon, S., Han, M., Wei, W., Chaudhuri, H., Yun, Y.-S., 2023. Facile and cost-effective fabrication of activated charcoal-carboxymethyl cellulose composite fiber for high-rate water-softening application. J. Ind. Eng. Chem. 126, 360–370. https://doi.org/10.1016/j.jiec.2023.06.025.

Ishikawa, S., Suyama, K., 1998. Recovery and refining of au by gold-cyanide ion biosorption using animal fibrous proteins. Appl. Biochem. Biotechnol. 70–72, 719–728. https://doi.org/10.1007/BF02920183.

Kim, C., Hong, H.-J., 2024. Recovery and isolation strategies of platinum, palladium, and rhodium from spent automotive catalyst leachate using a polyethylene-imine-grafted cellulose nanofibril aerogel. Ind. Eng. Chem. Res. 63, 4547–4556. https://doi.org/10.1021/acs.iecr.3c04137.

Lagergren, S., 1898. Zur Theorie der sogenannten Adsorption gelöster Stoffe. Bihang till Kungliga Svenska Vetenskapsakademiens Handlingar 24, 1–39.

Langmuir, I., 1916. The constitution and fundamental properties of solids and liquids. Part I solids. J. Am. Chem. Soc. 38, 2221–2295. https://doi.org/10.1021/ja02268a002.

Le Roux, C.J., Kriek, R.J., 2019. A detailed spectrophotometric investigation of the stability constants of [PdCln(OH)4-n]2− and [PdBrn(OH)4-n]2− (n = 0–4). Hydrometall. 186, 21–29. https://doi.org/10.1016/j.hydromet.2019.03.009.

Lever, A.B.P., 1974. Charge transfer spectra of transition metal complexes. J. Chem. Educ. 51, 612. https://doi.org/10.1021/ed051p612.

Li, Q., 2019. Progress in microbial degradation of feather waste. Front. Microbiol. 10, 2717. https://doi.org/10.3389/fmicb.2019.02717.

Luo, X., Huang, W., Mei, Y., Zhou, S., Zhu, L., 1999. Interaction of palladium(II) complexes with sulfur-containing peptides studied by electrospray mass spectrometry. Inorg. Chem. 38, 1474–1480. https://doi.org/10.1021/ic9805473.

Mahleba, M.M., Mukaba, J.-L., Tshentu, Z.R., 2025. Selective recovery of palladium (II) from acidic solutions using dithio- and benzimidazolylthio-functionalized resins. Minerals 15, 589. https://doi.org/10.3390/min15060589.

Maruyama, T., Terashima, Y., Takeda, S., Okazaki, F., Goto, M., 2014. Selective adsorption and recovery of precious metal ions using protein-rich biomass as efficient adsorbents. Process Biochem. 49, 850–857. https://doi.org/10.1016/j.procbio.2014.02.016.

Mattiello, S., Guzzini, A., Del Giudice, A., Santulli, C., Antonini, M., Lupidi, G., Gunnella, R., 2022. Physico-chemical characterization of keratin from wool and chicken feathers extracted using refined chemical methods. Polymers 15, 181. https://doi.org/10.3390/polym15010181.

Maurya, S.D., Singh, A., 2023. Application and future perspectives of keratin protein extracted from waste chicken feather: A review. Sustain. Chem. Eng. 32–46. https://doi.org/10.37256/sce.5120243521.

Mincke, S., Asere, T.G., Verheye, I., Folens, K., Vanden Bussche, F., Lapeire, L., Verbeken, K., Van Der Voort, P., Tessema, D.A., Fufa, F., Du Laing, G., Stevens, C.V., 2019. Functionalized chitosan adsorbents allow recovery of palladium and platinum from acidic aqueous solutions. Green Chem. 21, 2295–2306. https://doi.org/10.1039/C9GC00166B.

Molina, J.J., Lectez, S., Tazi, S., Salanne, M., Dufrêche, J.-F., Roques, J., Simoni, E., Madden, P.A., Turq, P., 2011. Ions in solutions: Determining their polarizabilities from first-principles. J. Chem. Phys. 134, 014511. https://doi.org/10.1063/1.3518101.

Murray, A.J., Zhu, J., Wood, J., Macaskie, L.E., 2017. A novel biorefinery: Biorecovery of precious metals from spent automotive catalyst leachates into new catalysts effective in metal reduction and in the hydrogenation of 2-pentyne. Miner. Eng. 113, 102–108. https://doi.org/10.1016/j.mineng.2017.08.011.

Nagarjuna, R., Sharma, S., Rajesh, N., Ganesan, R., 2017. Effective adsorption of precious metal palladium over polyethyleneimine-functionalized alumina nanopowder and its reusability as a catalyst for energy and environmental applications. ACS Omega 2, 4494–4504. https://doi.org/10.1021/acsomega.7b00431.

Nikoloski, A.N., Ang, K.-L., Li, D., 2015. Recovery of platinum, palladium and rhodium from acidic chloride leach solution using ion exchange resins. Hydrometall. 152, 20–32. https://doi.org/10.1016/j.hydromet.2014.12.006.

Nobahar, A., Carlier, J.D., Costa, M.C., 2023. Recovery of catalytic metals from leaching solutions of spent automotive catalytic converters using plant extracts. Clean Techn. Environ. Policy 25, 2707–2726. https://doi.org/10.1007/s10098-023-02523-1.

Nobahar, A., Carlier, J.D., Miguel, M.G., Costa, M.C., 2021. A review of plant metabolites with metal interaction capacity: A green approach for industrial applications. Biometals 34, 761–793. https://doi.org/10.1007/s10534-021-00315-y.

Paiva, A.P., Piedras, F.V., Rodrigues, P.G., Nogueira, C.A., 2022. Hydrometallurgical recovery of platinum-group metals from spent auto-catalysts – Focus on leaching and solvent extraction. Sep. Purif. Technol. 286, 120474. https://doi.org/10.1016/j.seppur.2022.120474.

Paul, S., Hewitt, A., Rana, S., Goswami, P., 2023. Development of novel parameters for characterising scale morphology of wool fibre and its correlation with dye diffusion coefficient of acid dye. Sci. Rep. 13, 18444. https://doi.org/10.1038/s41598-023-45689-w.

Petrov, A.I., 2024. Interaction of disulfides with metal ions and spectroscopic identification of the products. Coord. Chem. Rev. 505, 215678. https://doi.org/10.1016/j.ccr.2024.215678.

Petrov, A.I., 2023. Experimental and DFT study of the kinetics of the interaction of Pt(II) and Pd(II) with disulfides in hydrochloric acid solutions. Inorganica Chim. Acta 545, 121269. https://doi.org/10.1016/j.ica.2022.121269.

Polesca, C., Passos, H., Neves, B.M., Coutinho, J.A.P., Freire, M.G., 2023. Valorization of chicken feathers using aqueous solutions of ionic liquids. Green Chem. 25, 1424–1434. https://doi.org/10.1039/D2GC04477C.

Sadeghi, S., Dadashian, F., Eslahi, N., 2019. Recycling chicken feathers to produce adsorbent porous keratin-based sponge. Int. J. Environ. Sci. Technol. 16, 1119–1128. https://doi.org/10.1007/s13762-018-1669-z.

Saguru, C., Ndlovu, S., Moropeng, D., 2018. A review of recent studies into hydrometallurgical methods for recovering PGMs from used catalytic converters. Hydrometall. 182, 44–56. https://doi.org/10.1016/j.hydromet.2018.10.012.

Sahmoune, M.N., 2019. Evaluation of thermodynamic parameters for adsorption of heavy metals by green adsorbents. Environ. Chem. Lett. 17, 697–704. https://doi.org/10.1007/s10311-018-00819-z.

Saitoh, N., Nomura, T., Konishi, Y., 2017. Biotechnological Recovery of Platinum Group Metals from Leachates of Spent Automotive Catalysts, in: Kim, H., Alam, S., Neelameggham, N.R., Oosterhof, H., Ouchi, T., Guan, X. (Eds.), Rare Metal Technology 2017, The Minerals, Metals & Materials Series. Springer International Publishing, Cham, pp. 129–135. https://doi.org/10.1007/978-3-319-51085-9_13.

Sari, A., Mendil, D., Tuzen, M., Soylak, M., 2009. Biosorption of palladium(II) from aqueous solution by moss (Racomitrium lanuginosum) biomass: Equilibrium, kinetic and thermodynamic studies. J. Hazard. Mater. 162, 874–879. https://doi.org/10.1016/j.jhazmat.2008.05.112.

Sebben, D., Pendleton, P., 2015. Analysis of ionic strength effects on the adsorption of simple amino acids. J. Colloid Interface Sci. 443, 153–161. https://doi.org/10.1016/j.jcis.2014.12.016.

Shan, X., Shi, X., Tan, X., Pu, Y., Qiang, T., 2024. Valorization of waste feather fiber: One uranium resource recycling material. Nucl. Eng. Des. 429, 113596. https://doi.org/10.1016/j.nucengdes.2024.113596.

Shukla, M.K., Chauhan, B.V.S., Bhaskar, T., Dhar, A., Vedratnam, A., 2023. Recycling of Platinum Group Metals and Alternative Catalysts for Catalytic Converters, in: Upadhyay, R.K., Sharma, S.K., Kumar, V., Valera, H. (Eds.), Transportation Systems Technology and Integrated Management, Energy, Environment, and Sustainability. Springer Nature Singapore, Singapore, pp. 363–398. https://doi.org/10.1007/978-981-99-1517-0_17.

Sips, R., 1948. On the Structure of a Catalyst Surface. J. Chem. Phys. 16, 490–495. https://doi.org/10.1063/1.1746922.

Škerget, M., Čolnik, M., Zemljič, L.F., Gradišnik, L., Semren, T.Ž., Lovaković, B.T., Maver, U., 2023. Efficient and green isolation of keratin from poultry feathers by subcritical water. Polymers 15, 2658. https://doi.org/10.3390/polym15122658.

Solís-Moreno, C.A., Cervantes-González, E., Saavedra-Leos, M.Z., 2021. Use and treatment of chicken feathers as a natural adsorbent for the removal of copper in aqueous solution. J. Environ. Health Sci. Eng. 19, 707–720. https://doi.org/10.1007/s40201-021-00639-4.

Suyama, K., Fukazawa, Y., Suzumura, H., 1996. Biosorption of precious metal ions by chicken feather. Appl. Biochem. Biotechnol. 57–58, 67–74. https://doi.org/10.1007/BF02941689.

Temkin, M., Pyzhev, V., 1940. Kinetics of ammonia synthesis on promoted iron catalysts. Acta Physicochim. URSS 12, 327–356.

Tesfaye, T., Sithole, B., Ramjugernath, D., 2017. Valorisation of chicken feathers: a review on recycling and recovery route—current status and future prospects. Clean Techn. Environ. Policy 19, 2363–2378. https://doi.org/10.1007/s10098-017-1443-9.

The Business Research Company, 2025. Automotive catalytic converter global market report.

Trinh, H.B., Lee, J.-C., Suh, Y., Lee, J., 2020. A review on the recycling processes of spent auto-catalysts: Towards the development of sustainable metallurgy. Waste Manag. 114, 148–165. https://doi.org/10.1016/j.wasman.2020.06.030.

Turanov, A.N., Karandashev, V.K., Artyushin, O.I., Sharova, E.V., Genkina, G.K., 2017. Adsorption of palladium(II) from hydrochloric acid solutions using polymeric resins impregnated with novel N-substituted 2-(diphenylthiophosphoryl)acetamides. Sep. Purif. Technol. 187, 355–364. https://doi.org/10.1016/j.seppur.2017.06.068.

Vasile, E., Ciocanea, A., Ionescu, V., Lepadatu, I., Diac, C., Stamatin, S.N., 2021. Making precious metals cheap: A sonoelectrochemical – Hydrodynamic cavitation method to recycle platinum group metals from spent automotive catalysts. Ultrason. Sonochem. 72, 105404. https://doi.org/10.1016/j.ultsonch.2020.105404.

Wang, Z., Kang, S., Won, S., 2021. Recovery of Pd(II) from aqueous solution by polyethylenimine-crosslinked chitin biosorbent. Coatings 11, 593. https://doi.org/10.3390/coatings11050593.

Weber, W.J., Morris, J.C., 1963. Kinetics of adsorption on carbon from solution. J. Sanit. Eng. Div. 89, 31–59. https://doi.org/10.1061/JSEDAI.0000430.

Weißpflog, J., Gündel, A., Vehlow, D., Steinbach, C., Müller, M., Boldt, R., Schwarz, S., Schwarz, D., 2020. Solubility and selectivity effects of the anion on the adsorption of different heavy metal ions onto chitosan. Molecules 25, 2482. https://doi.org/10.3390/molecules25112482.

Wołowicz, A., Hubicki, Z., 2024. Evaluation of adsorption ability of Lewatit® VP OC 1065 and Diaion™ CR20 ion exchangers for heavy metals with particular consideration of palladium(II) and copper(II). Molecules 29, 4386. https://doi.org/10.3390/molecules29184386.

Wołowicz, A., Hubicki, Z., 2012. The use of the chelating resin of a new generation Lewatit MonoPlus TP-220 with the bis-picolylamine functional groups in the removal of selected metal ions from acidic solutions. Chem. Eng. J. 197, 493–508. https://doi.org/10.1016/j.cej.2012.05.047.

Won, S.W., Yun, Y.-S., 2013. Recovery of metallic palladium from hydrochloric acid solutions by a combined method of adsorption and incineration. Chem. Eng. J. 218, 303–308. https://doi.org/10.1016/j.cej.2012.12.052.

Xia, J., Ghahreman, A., 2023. Platinum group metals recycling from spent automotive catalysts: Metallurgical extraction and recovery technologies. Sep. Purif. Technol. 311, 123357. https://doi.org/10.1016/j.seppur.2023.123357.

Yakoumis, I., Moschovi, A.M., Giannopoulou, I., Panias, D., 2018. Real life experimental determination of platinum group metals content in automotive catalytic converters. IOP Conf. Ser.: Mater. Sci. Eng. 329, 012009. https://doi.org/10.1088/1757-899X/329/1/012009.

Yousif, A.M., 2019. Recovery and then individual separation of platinum, palladium, and rhodium from spent car catalytic converters using hydrometallurgical technique followed by successive precipitation methods. J. Chem. 2019, 1–7. https://doi.org/10.1155/2019/2318157.

Zamri, N.I.I., Zulmajdi, S.L.N., Daud, N.Z.A., Mahadi, A.H., Kusrini, E., Usman, A., 2021. Insight into the adsorption kinetics, mechanism, and thermodynamics of methylene

blue from aqueous solution onto pectin-alginate-titania composite microparticles. SN Appl. Sci. 3, 222. https://doi.org/10.1007/s42452-021-04245-9.
Zhang, L.i., Li, B., Shao, P., Zhou, X., Li, D., Hu, Z., Dong, H., Yang, L., Shi, H., Luo, X., 2023a. Selective capture of palladium from acid wastewater by thiazole-modified activated carbon: Performance and mechanism. Environ. Res. 238, 117253. https://doi.org/10.1016/j.envres.2023.117253.
Zhang, L., Ren, J., Bai, W., 2023b. A review of poultry waste-to-wealth: Technological progress, modeling and simulation studies, and economic- environmental and social sustainability. Sustainability 15, 5620. https://doi.org/10.3390/su15075620.
Zhang, X., Chen, Z., Wan, Z., Liu, C., He, R., Xie, X., Huang, Z., 2022. Selective recovery of palladium (II) from metallurgical wastewater using thiadiazole-based chloromethyl polystyrene-modified adsorbent. Int. J. Mol. Sci. 23, 12158. https://doi.org/10.3390/ijms232012158.